

# MedGNN: Capturing the Links Between Urban Characteristics and Medical Prescriptions

MINWEI ZHAO, University College London, UK

SANJA SCEPANOVIC, Nokia Bell Labs, U.K., UK

STEPHEN LAW, University College London, UK

DANIELE QUERCIA, Nokia Bell Labs, U.K., UK

IVICA OBADIC, Technical University of Munich, Germany

Understanding how urban socio-demographic and environmental factors relate with health is essential for public health and urban planning. However, traditional statistical methods struggle with nonlinear effects, while machine learning models often fail to capture geographical (nearby areas being more similar) and topological (unequal connectivity between places) effects in an interpretable way. To address this, we propose MedGNN, a spatio-topologically explicit framework that constructs a 2-hop spatial graph, integrating positional and locational node embeddings with urban characteristics in a graph neural network. Applied to MEDSAT, a comprehensive dataset covering over 150 environmental and socio-demographic factors and six prescription outcomes (depression, anxiety, diabetes, hypertension, asthma, and opioids) across 4,835 Greater London neighborhoods, MedGNN improved predictions by over 25% on average compared to baseline methods. Using depression prescriptions as a case study, we analyzed graph embeddings via geographical principal component analysis, identifying findings that: align with prior research (e.g., higher antidepressant prescriptions among older and White populations), contribute to ongoing debates (e.g., greenery linked to higher and  $\text{NO}_2$  to lower prescriptions), and warrant further study (e.g., canopy evaporation correlated with fewer prescriptions). These results demonstrate MedGNN’s potential, and more broadly, of carefully applied machine learning, to advance transdisciplinary public health research.

## 1 Introduction

Public health research examines socio-demographic and environmental characteristics as key drivers of urban health outcomes and inequalities [28, 38]. Given the rapidly changing global landscape [46], including urbanization [114], frequent occurrence of extreme weather events [10], and the outbreaks and pandemics such as COVID-19 [21], urban policymakers and health administrators have also been pressed with the need for systematic research on the relationships between urban characteristics and health [30, 91].

Previous public health and urban studies have achieved varying degrees of success using traditional statistical methods [4, 31, 51], and machine learning models [33, 82, 116]. However, statistical approaches struggle with nonlinear effects, while machine learning models often fail to capture spatial relationships (e.g., how close neighborhoods are to each other, and geographic barriers like roads or rivers) and topological relationships (e.g., how connected neighborhoods are despite their physical distance), reducing predictive accuracy [56]. To address these issues, we need not only to learn the relationships between environmental and socio-demographic features with health outcomes, exemplified with traditional statistical methods, but also to model and uncover the nonlinear spatial and topological dependencies between places. Graph neural networks (GNNs), effective for modelling graph-structured data, have had a wide-ranging impact in fields like social network analysis, molecular chemistry, and recommendation systems [75, 107, 121]. Previous urban science research [77, 125] demonstrated the usefulness of GNNs for encoding spatial

---

Authors’ Contact Information: Minwei Zhao, minwei.zhao.22@ucl.ac.uk, University College London, London, UK; Sanja Scepanovic, Nokia Bell Labs, U.K., Cambridge, UK, sanja.scepanovic@nokia-bell-labs.com; Stephen Law, University College London, London, UK, stephen.law@ucl.ac.uk; Daniele Quercia, Nokia Bell Labs, U.K., Cambridge, UK, daniele.quercia@nokia-bell-labs.com; Ivica Obadic, Technical University of Munich, Munich, Germany, ivica.obadic@tum.de.

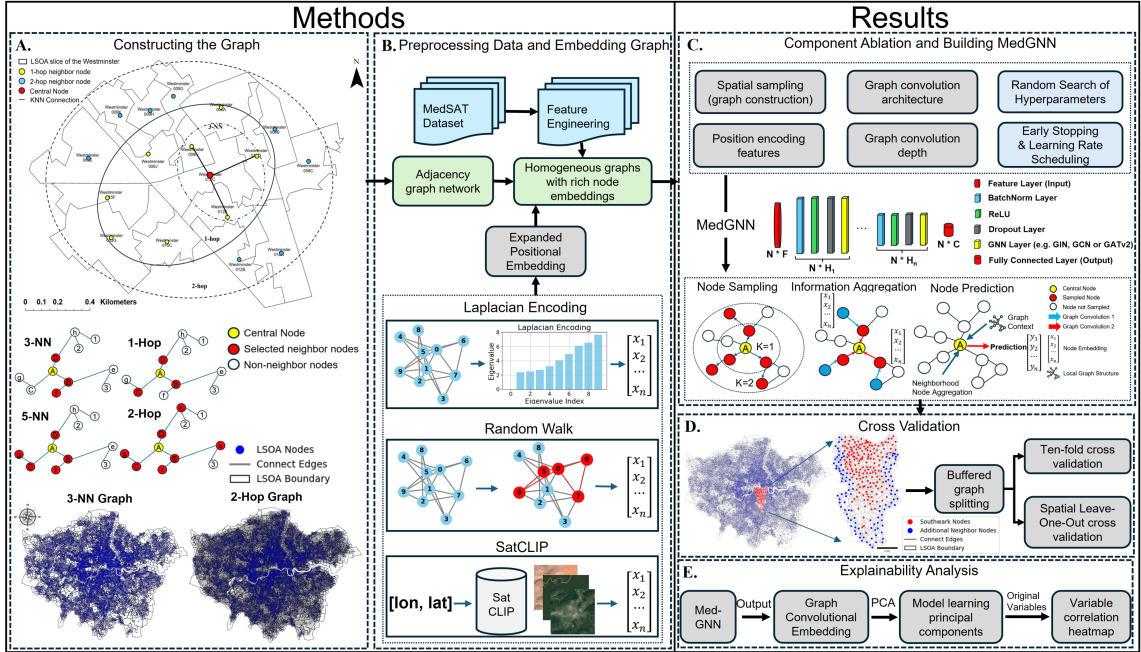


Fig. 1. Our methodology involves five key steps: (A) Constructing an adjacency graph from LSOA geographic locations using K-Hop [23] and KNN [37] methods; (B) Preprocessing MedSAT features into node embeddings, and incorporating Laplacian encoding [34], random walk encoding [100], or SatCLIP location encoding [64] and their combinations; (C) Developing MedGNN via component ablation, illustrating its architecture, aggregation, update mechanisms, and subgraph-based predictions; (D) Cross-validation (CV) of training and testing graphs in both 10-fold and leave-one-out CV; and (E) Conducting explainability analysis by interpreting MedGNN graph embeddings to reveal correlations between prescription patterns and city characteristics through heatmaps and visualizations.

dependency, and heterogeneity in predicting traffic flows and urban functions respectively. However, despite their successes in various domains, the effectiveness of GNNs in public health applications remains under-explored, partly due to their limited interpretability [63, 78]. To tackle this gap, and respond to recent calls for more research on machine learning and AI in public health [66, 86], we proposed a novel GNN framework that captures the spatial and topological dependencies between socio-demographic features and health outcomes at the neighbourhood level, and we also conducted a geographical explainability analysis to interpret these complex factors in a spatially robust manner. In doing so, we made three key contributions:

- (1) We proposed MedGNN, a novel framework that encodes spatial and topological dependencies between geographical areas to estimate health outcomes as a node prediction problem. We conducted extensive spatial ablation, testing various spatial graph constructions ( $k$ -hop and  $k$ -NN), positional encodings (Laplacian, random walk, SatCLIP), and GNN architectures (GCN, GIN, GraphSAGE, GATv2) to develop MedGNN, providing a reference pipeline for related research in this area (§3.1).
- (2) We applied MedGNN on a recent MedSAT dataset [116] that integrates high-resolution environmental indicators like air quality, greenness, climate characteristics, and socio-demographic attributes like ethnicity and age, with health outcome indicators such as per capita medical prescription quantities for depression. MedGNN achieved significantly higher accuracy with an average improvement of over 25% across the 6 prescription outcomes compared

to baseline models from previous studies, such as LightGBM, the Spatial Lag Model (SLM), and Geographically Weighted Regression (GWR) [82, 116], confirming its superior ability to capture nonlinear spatial and topological relationships (§3.2).

- (3) Lastly, using depression (one of the key health issues nowadays in England [36, 108] and beyond [12]) as a case study, we demonstrated how geographic explainability analysis can be performed on MedGNN to confirm existing and uncover insights calling for future research. We correlated the PCA dimensions of MedGNN’s embeddings with various neighbourhood features. The results largely aligned with previous research (e.g., older age and White population being associated with more antidepressants), some added to the existing debates (e.g., greenery being associated with more and NO<sub>2</sub> with less antidepressants), and some are insights not previously reported that call for future research (e.g., canopy evaporation associated with less prescriptions), highlighting MedGNN’s potential to support public health research (§3.3).

## 2 Methods and Data

Our framework consists of the five main steps shown in Figure 1.

### 2.1 Constructing the Graph

To cast the problem of predicting prescription outcomes in geographical neighbourhoods as a node prediction task in a graph neural network, we represented the geographic distribution of LSOAs as a graph  $G = (\mathcal{V}, \mathcal{E})$ , where each LSOA  $v_i \in \mathcal{V}$  is a node, positioned at the centroid of the neighbourhood, and each edge  $e_{ij} \in \mathcal{E}$  represents the adjacency relationship between LSOAs, as defined by the adjacency matrix  $A$ . Each node has its corresponding initial feature vector  $h_i^{(0)}$  and prescription target  $y_i$ . Part A of Figure 1 illustrates this process. Different definitions of adjacency can result in distinct graphs. Therefore, determining the optimal adjacency type to best capture spatial representation is a key challenge addressed in the ablation study conducted in Step 3. (shown in Part C of Figure 1).

### 2.2 Preprocessing Data and Embedding Graph

**2.2.1 MedSAT.** MedSAT integrates detailed socio-demographic and environmental indicators at the LSOA level for 2019 and 2020, with this study focusing on 2020 data in London. Compiling data from Office for National Statistics [40], National Health Services [90], and remote sensing platforms like Copernicus and Google Earth Engine [45], MedSAT ensures consistency and accuracy across variables [116]. It includes 111 socio-demographic indicators (e.g., gender ratio, age distribution, poverty), and 55 environmental variables (air quality, greenery, landcover, climate). Additionally, it provides six per capita prescription outcomes (i.e., anxiety, depression, diabetes, hypertension, asthma, and opioids) sourced from NHS records, enabling detailed analyses of health, socio-demographic, and environmental relationships.

**2.2.2 Preprocessing.** The LSOA features provided by MedSAT are embedded as node attributes in the graph. To ensure robust modelling and reliable prediction outcomes, preprocessing steps were performed on the MedSAT to address dimensionality and multicollinearity issues before embedding. These steps included exploratory analyses using a correlation matrix, visual inspections of individual variables, and feature selection through Variance Inflation Factor (VIF) iteration [11, 22, 69, 95]. We first identified highly correlated variables using a correlation matrix, and selected the most representative ones among them through visual inspection. To address high dimensionality while retaining complex relationships [44], we sequentially selected variables based on a VIF threshold (VIF<1000) and higher tolerance for fixed variables (Table 3 of Appendix A) (VIF<1500) [1]. This threshold ensured a balance between reducing redundant

information and preserving sufficient data complexity for capturing intricate dependencies. The iterative process for VIF-based feature selection works by first calculating the VIF values for all features. Features with high VIF values, indicating strong multicollinearity, were identified and removed one by one. After each removal, the VIF values were recalculated for the remaining features, and the process continued until all remaining features had VIF values below the set threshold.

Before the VIF iteration process, a set of commonly used control variables in public health research was pre-selected and fixed in the model. These fixed variables serve as foundational controls to account for known confounders in health outcome studies [17, 29, 49, 53, 55]. Finally, the preprocessed MedSAT data following the above feature engineering steps, was embedded into each LSOA as node attributes.

**2.2.3 Positional Encoding.** In addition to node embeddings from preprocessed MedSAT, we applied positional encoding to add more detailed topological and spatial description for each node. The encoding methods are also a subject of the ablation process in Step C (Figure 1). We tested two position encodings and one location encoding method and their combinations to improve the graph’s local information richness [24, 65, 81, 117]. A novelty of the research is the integration of both positional and locational encoding as node attributes, enabling the model to capture relational and absolute spatial dependencies. For detailed processes of position encoding, see Appendix C.4.

**Laplacian Position Encoding.** Among them, the Laplacian position encoding method embeds the position by combining node features with the graph’s Laplacian matrix using spectral methods. It provides geometric information of the local graph structure by capturing the smoothness of the graph structure [34].

**Random Walk Position Encoding.** Random walk learns node representations by simulating random walk paths of nodes in a graph [34]. Each random walk process gives a path from one node to another, which helps encode the relative positions of nodes and capture the local structural information between nodes [34, 123]. Since the local subgraph is characterized by relatively simple adjacency relationships, only a single random walk process was embedded for each node.

**SatCLIP Location Encoding.** SatCLIP proposed by Klemmer et al. [64], is a location encoding method that combines satellite images (Sentinel-2) with geographic coordinates. The pretrain GeoAI model embeds both image and geographical information into a shared representation, generating a 256-dimensional location encoding. To ensure computational efficiency, we applied Principal Component Analysis (PCA) to reduce the dimensionality of the location embeddings.

## 2.3 Performing Component Ablation and Building MedGNN

**2.3.1 MedGNN.** After constructing the spatial graphs, various socio-demographic and environmental characteristics of LSOAs were embedded as node attributes. Through multiple graph convolution operations, information was iteratively aggregated, enabling node features to capture structural and neighbourhood influences. Finally, node embeddings were mapped to the prediction space of health outcomes via a fully connected layer (Figure 1 E). More formally, the objective of MedGNN is to learn a  $GNN : H^{(0)} \rightarrow Y$  that maps input node features to prescription outcomes by leveraging both graph-based and spatial dependencies to minimise the Mean Squared Error (MSE) between the actual and predicted prescriptions. This is given by  $\mathcal{L} = \frac{1}{N} \sum_{i=1}^N (y_i - \hat{y}_i)^2$ , where  $N$  is the number of nodes,  $y_i$  is the target prescription outcome, and  $\hat{y}_i$  is the predicted value obtained from the model.

**2.3.2 Component Ablation.** To evaluate the effectiveness of different components in MedGNN, we conducted an ablation study by systematically testing the impact of different parameters and component layers using the validation set [60, 85]. All ablation tests were conducted using a 3-fold cross-validation on the training data with a 80:20 data

resampling. The optimal learning rate (0.001), optimizer (Adam), training epochs (300) and other parameter combinations were determined through 10 rounds of random search [2] within the standard GNN hyper-parameter space [126]. In addition to evaluating different spatial representation and position encoding methods mentioned in steps A and B (Figure 1), we also performed ablation experiments on the graph convolutional architectures and model depths. We tested four GNNs — Graph Convolution Networks (GCN), Graph Isomorphism Networks (GIN), GraphSAGE and Graph Attention Networks v2 (GATv2) [15, 48, 124]. These different GNNs have different ways of aggregating information on graphs (see Appendix C.3 for more details).

## 2.4 Cross Validation

To ensure robust evaluation of MedGNN, we employed two random cross-validation strategies: a 10-fold cross-validation [43] and a modified leave-one-out cross-validation (LOOCV) [119]. Given the graph-based nature of the data, splitting the graph into training and testing subsets posed unique challenges. Improper resampling could lead to spatial data leakage or graph fragmentation, where the structural relationships between nodes are broken, affecting model performance.

*2.4.1 Ten-fold Cross Validation.* For 10-fold cross-validation, we divided the graph into 10 subgraphs, ensuring that each test subgraph maintained connectivity, and included all nodes within a 2-hop buffer from the test nodes. This approach, illustrated in Figure 1 D, ensures that test nodes are surrounded by sufficient context from their neighborhood, preventing disconnection from the graph structure.

*2.4.2 Leave-One-Out Cross-Validation.* It is a robust evaluation method in which each instance in the dataset is used as a test set while the remaining instances serve as the training set [119]. We implemented geographically distributed LOOCV by isolating specific regions within London, such as Southwark, as the test set while utilizing the other LSOA nodes for training. This method allowed to evaluate the model’s spatial generalization capabilities to previously ‘unseen data’, highlighting local effects and reducing the risks of spatial data leakage [72]. Given the computational complexity, and the large size of the graph, we selected six representative Boroughs across London, and performed LOOCV on their contained LSOAs (Figure 5). This strategy ensured a manageable computational cost while capturing diverse geographic and socio-demographic locations, graph structures, and node relationships, supporting model generalizability. The graph splitting for the LOOCV process is consistent with the splitting algorithm of the 10-fold cross validation. Part D of Figure 1 presents an example where the Borough of Southwark in London is set as a test subgraph. Both 10-fold CV and LOOCV included metrics like root mean square error (RMSE), mean absolute error (MAE), and  $R^2$  score to evaluate CV performance. The parameter sets used for cross-validation were obtained through 50 rounds of random search.

## 2.5 Explainability Analysis

To understand the relationship between the socio-demographic and environmental characteristics learned by MedGNN and the health prescription results, we applied PCA [47] on the embeddings generated from MedGNN. PCA reduced the high-dimensional embeddings into orthogonal principal components, simplifying their interpretation and enabling a direct examination of feature importance. For a given prescription outcome, we identified principal components explaining over 80% of the variance [27]. Next, we visualised the components geographically and calculated the Pearson correlation coefficients between the principal components and the original input features, quantifying the relationship between the embeddings and the socio-demographic and environmental factors in the dataset. This geographical explainability approach bridges the gap between complex graph-based representations and health outcomes, providing transparency and interpretability in model predictions.

Table 1. Ten-fold cross-validation of MedGNN. Its  $R^2$  scores are compared against two statistical baselines (SLM and GWR) and one machine learning method (LightGBM) across six health outcomes. While SLM and GWR were directly fitted to the data, LightGBM also underwent cross-validation. Best results are highlighted in bold and runner-up results are underlined.

Model	Diabetes	Hypertension	Asthma	Depression	Anxiety	Opioids
SLM	0.711	0.725	0.684	0.714	0.678	0.677
GWR	<u>0.726</u>	<u>0.752</u>	<u>0.710</u>	<u>0.734</u>	<u>0.705</u>	<u>0.691</u>
LightGBM	0.632 $\pm$ 0.029	0.649 $\pm$ 0.017	0.589 $\pm$ 0.024	0.628 $\pm$ 0.020	0.586 $\pm$ 0.021	0.535 $\pm$ 0.032
MedGNN (Ours)	<b>0.900 <math>\pm</math> 0.009</b>	<b>0.915 <math>\pm</math> 0.013</b>	<b>0.896 <math>\pm</math> 0.007</b>	<b>0.915 <math>\pm</math> 0.010</b>	<b>0.911 <math>\pm</math> 0.009</b>	<b>0.902 <math>\pm</math> 0.013</b>
<b>Percentage Increase (from GWR)</b>	23.83%	21.59%	26.05%	24.69%	29.20%	30.55%

Component Ablation	Message Passing Mechanism				Adjacency Matrix Construction			Depth			Position encoding			3-fold R2 for Depression		
	GCN	GIN	GraphSAGE	GATv2	3-NN	5-NN	1-HOP	2-HOP	3-HOP	1	2	3	Laplace		SatCLIP	Random Walk
GATv2 was selected as the optimal architecture	√						√					√				0.719 $\pm$ 0.009
		√					√					√				0.782 $\pm$ 0.020
			√				√					√				0.735 $\pm$ 0.006
				√*			√					√				0.871 $\pm$ 0.008
1-HOP was selected as the optimal spatial representation				√*		√						√				0.856 $\pm$ 0.002
				√*		√						√				0.867 $\pm$ 0.005
				√*		√*						√				0.871 $\pm$ 0.008
				√*			√					√				0.871 $\pm$ 0.004
The optimal depth of the model is 2				√*				√				√*				0.723 $\pm$ 0.002
				√*				√*				√*				0.871 $\pm$ 0.008
				√*				√*				√				0.762 $\pm$ 0.011
				√*			√*					√*				0.871 $\pm$ 0.008
The optimal position encoding is a combination of Random Walk and SatCLIP				√*				√*				√*			√*	0.877 $\pm$ 0.003
				√*				√*				√*			√*	(1-D embedding)
				√*				√*			√	√*				0.872 $\pm$ 0.008(3-D)
				√*				√*				√*				0.874 $\pm$ 0.004(1-D)
Optimal *				√*				√*				√*				0.887 $\pm$ 0.002(2-D)
				√*				√*			√	√*			√*	0.884 $\pm$ 0.005(3-D)
				√*				√*			√	√*				0.880 $\pm$ 0.004(3+2-D)
				√*				√*				√*				0.897 $\pm$ 0.005(2+2-D)

\*Indicates the first determination of this type of component

Fig. 2. Spatial Component Ablation Study Table for MedGNN Construction.

### 3 Results

#### 3.1 Component Ablation

Figure 2 presents all ablation processes, interim results, and the final configuration of MedGNN. With  $R^2$  as the evaluation metric, we sequentially determined the optimal components: model architecture, spatial representation, depth, and position embedding approach. We first selected the GatV2 for the architecture, followed by a 2-hop spatial adjacency graph, a 2-layer graph convolution depth, and finally, the position embedding combination of Random Walk and SatCLIP. It is worth noting that when choosing the spatial representation method, there is only a slight performance improvement for 2-hop and 3-hop methods compared to 1-hop, and considering the computational cost, we chose the 1-hop method.

#### 3.2 Cross Validation

**3.2.1 Ten-fold Cross-Validation.** Table 1 compares the prediction performance of MedGNN under 10-fold cross-validation across six medical prescription types against three baseline models (SLM, LightGBM, and GWR). Details of the three baseline models can be found in the Appendix C.2. MedGNN consistently achieved highest  $R^2$  scores across all health outcomes, significantly outperforming all baseline models (average performance increase of over 25%), with the largest improvements for anxiety, depression, and opioid use. For depression, we also conducted a spatial residual analysis and visualized the predicted and actual prescription rates per capita across London. These analyses provide

Table 2. LOOCV evaluation of MedGNN. Each of six Boroughs serves as a test set, with metrics for six health outcomes.

		Camden	Barking	Barnet	Southwark	Croydon	Ealing	Average
Diab.	RMSE	3.929	7.025	6.829	5.611	4.604	10.427	6.404
	MAE	2.798	5.277	4.839	4.107	3.344	6.799	4.527
	$R^2$	0.779	0.883	0.829	0.803	<b>0.898</b>	0.794	0.831
Hyper.	RMSE	6.701	12.337	9.881	8.511	7.117	11.636	9.364
	MAE	4.554	7.863	6.807	5.693	5.166	7.309	6.232
	$R^2$	0.832	0.815	0.868	0.843	<b>0.925</b>	0.732	0.836
Asth.	RMSE	1.144	1.545	1.409	1.494	1.251	1.621	1.411
	MAE	0.872	1.031	0.925	1.126	0.893	1.108	0.993
	$R^2$	0.759	0.821	0.836	0.764	<b>0.883</b>	0.737	0.800
Depr.	RMSE	1.975	2.532	2.535	2.629	2.815	2.678	2.527
	MAE	1.374	1.891	1.654	1.899	1.743	1.842	1.734
	$R^2$	0.888	<b>0.901</b>	0.881	0.873	0.884	0.771	0.866
Anxi.	RMSE	3.811	3.702	4.270	3.830	3.488	4.494	3.933
	MAE	2.391	2.701	2.865	2.828	2.317	2.821	2.654
	$R^2$	0.808	0.887	0.843	0.866	<b>0.903</b>	0.745	0.842
Optio.	RMSE	1.440	2.284	1.623	1.992	1.982	1.629	1.825
	MAE	0.943	1.495	1.090	1.365	1.446	1.134	1.246
	$R^2$	0.832	0.839	0.846	0.768	<b>0.888</b>	0.759	0.822

insights into the model’s ability to capture spatial variability and highlight regions with potential systematic errors.

**Predicted vs. Real Values.** Figure 3 shows the predicted (bottom-left) and actual (bottom-right) number of depression prescriptions per capita for each LSOA in London. The maps use a color gradient to represent prescription rates, with blue indicating lower rates and red indicating higher rates. The missing data areas, such as certain LSOAs where prescription data is unavailable, are marked in black. These maps show how MedGNN effectively captures the general spatial trends of depression prescriptions. High-prescription regions (e.g., Southeast London) and low-prescription regions (e.g., Central London) are correctly identified in the predictions. However, some areas show discrepancies, particularly in regions with sparse nodes (large-area LSOAs) or unique socio-demographic characteristics (e.g., the southeast and northwest suburbs of London). Even with such differences, the predicted values show a very similar distribution trend as the true values.

**Residuals Distribution.** The top panel of Figure 3 illustrates the absolute residuals of the predictions, highlighting areas where the model overestimates or underestimates prescription rates. The histogram inset shows the distribution of residuals, with a mean of  $-0.2246$ , and a standard deviation of  $1.9008$ . The relatively narrow distribution and low mean residual value indicate that the model performs consistently across most regions. Spatially, residuals with larger values were more concentrated in Central and East London. These regions likely reflect local socio-demographic and environmental factors not fully captured by the MedSAT dataset or model adjacency relationships. This suggests that while MedGNN effectively generalizes across the city, local refinements or additional features could improve performance in these regions.

**3.2.2 Leave-One-Out Cross-Validation.** We performed LOOCV on six Boroughs in London—Camden, Barking, Barnet, Southwark, Croydon and Ealing (see Figure 5 in Appendix C.1)—chosen for their diverse geographic, socio-demographic and environmental characteristics [59, 89]. Table 2 summarizes the LOOCV results, which offer a stricter evaluation than random cross-validation by testing on whole unseen regions. Compared to 10-fold CV, MedGNN’s  $R^2$  scores show

a slight decline across all outcomes, with most varying by less than 0.1. For diabetes, however, we observe a sharper drop—especially in Camden and Ealing—yet MedGNN still achieves an average  $R^2$  of above 0.8. Similarly, the results for Camden, Southwark and Ealing also show significant declines for asthma, suggesting that these areas may have more complex drivers of chronic diseases or greater urban heterogeneity. It is also evident that predicting certain regions (e.g., Croydon) is easier than others. Despite the expected reductions compared to 10-fold cross-validation, MedGNN still outperforms the baseline models (SLM, LightGBM, and GWR) evaluated under the easier 10-fold setting (Table 1), demonstrating its ability to capture complex spatio-topological relationships also under this more challenging validation scenario.

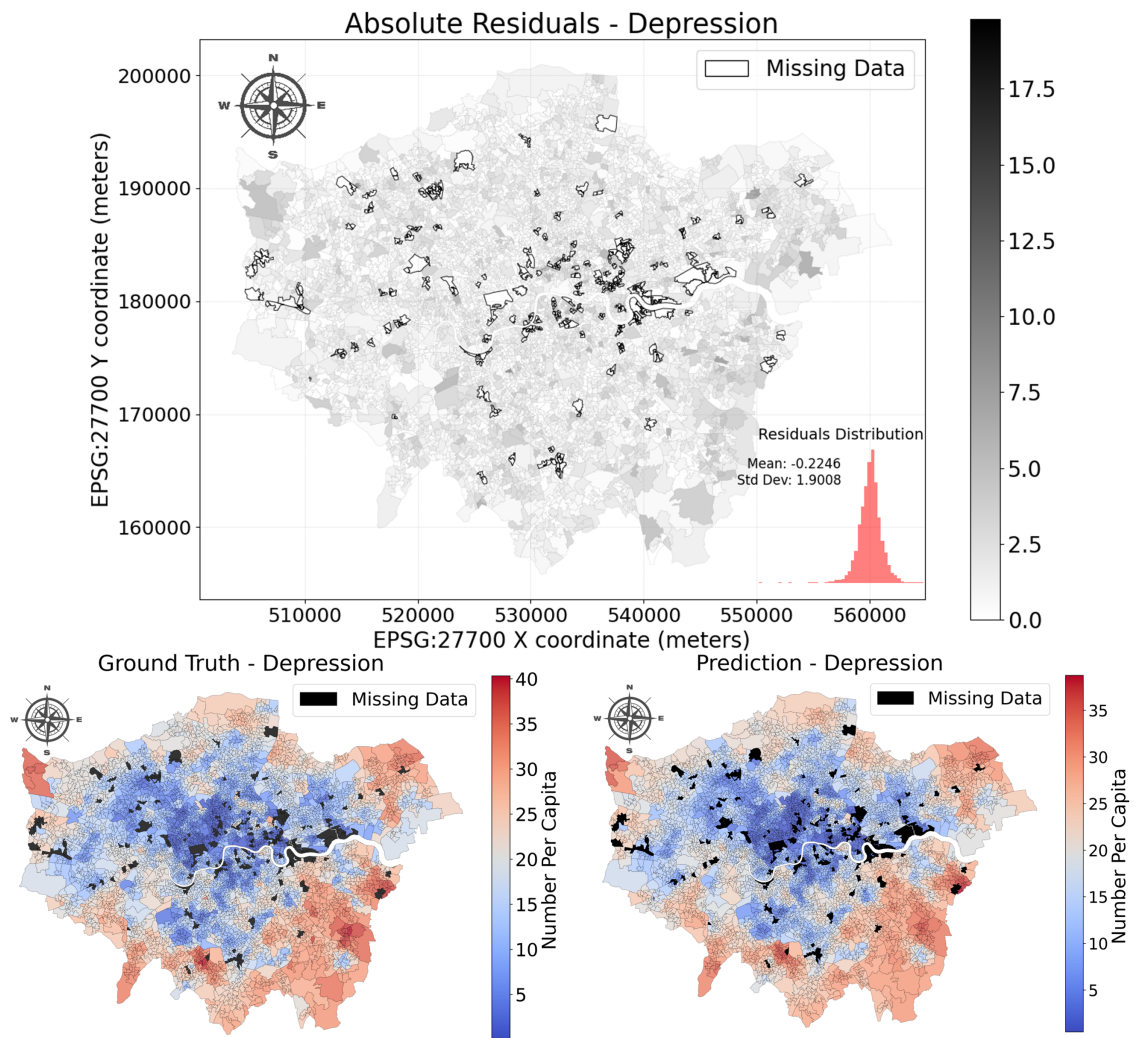


Fig. 3. Spatial residual analysis on the example of Antidepressants prediction. The figure illustrates (top) absolute residuals, (bottom-left) actual values, and (bottom-right) the spatial distribution of predicted values, offering insights into spatial heterogeneity and model performance.

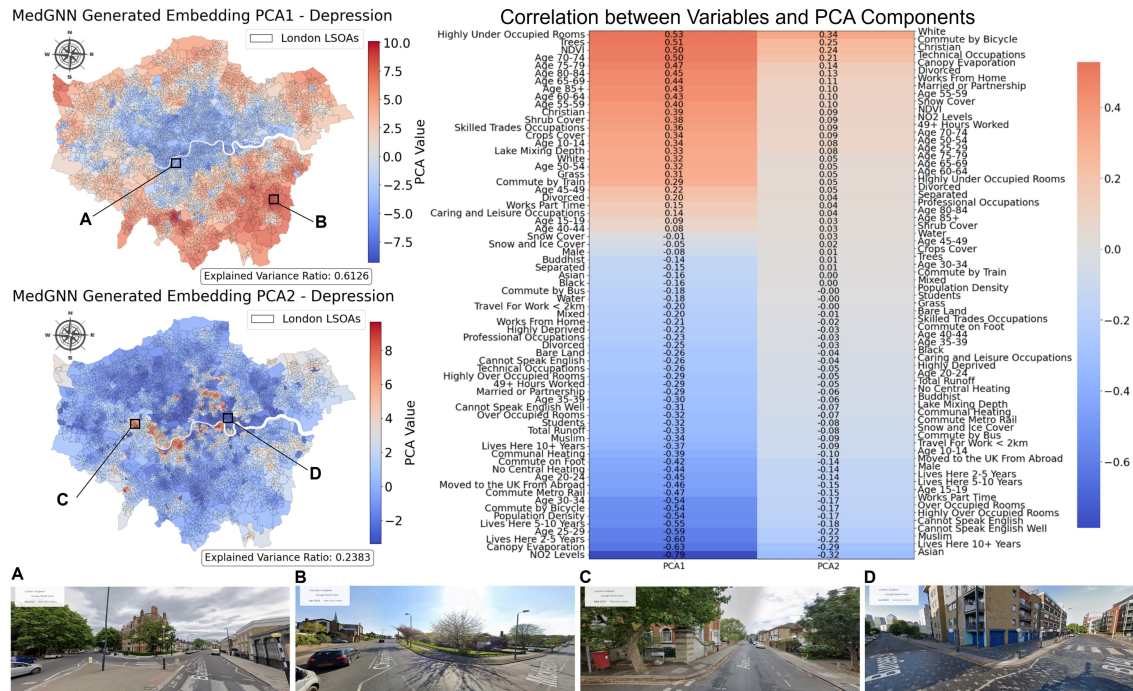


Fig. 4. (A) Spatial distribution of PCA1 values for depression embeddings. (B) Spatial distribution of PCA2 values. (C) Correlation heatmap between PCA components and input features. (D) Example street views of selected LSOAs.

### 3.3 Explainability Analysis

Figure 4 illustrates that the first two principal components (PCA1 and PCA2) explain 61.26% and 23.83% of the variance, in depression prescription embeddings, respectively. Left part of Figure 4 illustrates the spatial distribution of PCA1 and PCA2 values across London LSOAs. PCA1 captures global spatial trends, with lower values in central London (e.g., Region A) and higher values in peripheral areas (e.g., Region B). This spatial representation aligns with urbanization gradients and socio-demographic disparities. In contrast, PCA2 highlights more localized variations, with significant differences between specific neighbourhoods (e.g., Regions C and D). This component appears to capture fine-grained relationships between environmental features (e.g., green spaces), specific community living environment differences (e.g., main ethnic groups and religious beliefs of residents), and mental health outcomes.

To interpret the PCA components, we calculated the Pearson correlation coefficients between each principal component and the original input features (the heatmap in Figure 4). We found strong correlations with socio-demographic factors such as population density (-0.54), air pollution (-0.79), housing deprivation (0.53), and income levels (-0.23) indicating that PCA1 primarily reflects urbanization level and socio-demographic status gradients. In addition, we also found that this principal component has a significant age-related trend. Younger population tends to be in the city center, while the elderly population is distributed in the periphery of the city. As for PCA2, it exhibits notable correlations with several environmental and demographic features, highlighting its role in capturing complex localised patterns that influence prescription use. Specifically, PCA2 shows relationships with ethnic composition, including a

positive correlation with the percentage of White residents (0.34) and a negative correlation with the percentage of Asian residents (-0.32) on the opposite spectrum. Additionally, PCA2 is moderately associated with indices of religious diversity, such as a positive correlation with Christian beliefs (0.24), and a negative correlation with Muslim beliefs (-0.22). These insights suggest the importance of considering cultural diversity when analysing urban health disparities, and designing community-focused interventions. Environmental factors also play a significant role, as evidenced by the positive correlations with NDVI in both components, which indicate that areas with higher vegetation levels (e.g., green spaces) are more positively represented by those components. Moreover, socio-demographic aspects such as housing conditions (e.g., heating availability) and commuting patterns further contribute to the variability captured by PCA2, suggesting its relevance in reflecting localised living environment characteristics and their relationships with prescriptions.

## 4 Discussion

### 4.1 MedGNN

MedGNN significantly surpasses all baselines in predictive performance on medical prescriptions, confirming its enhanced ability to capture spatial and topological dependencies and heterogeneity. Specifically, we demonstrated that MedGNN allowed for more expressive aggregation, providing a deeper understanding of spatial relationships within the data, which led to significantly more accurate predictions than simpler, spatial regression and machine learning baselines. As previous research argues, *“if a model approximates the data generating process well enough, its interpretation should reveal better insights into the underlying process”*, i.e., in our case, into the drivers of medical prescriptions [87]. We also proposed a novel approach for feature engineering. While previous studies have addressed multicollinearity by selecting variables based on VIF thresholds and mutual information [25], many interdisciplinary studies overlook redundancy among input variables. For example, studies on anxiety disorders and air pollution [111], or on urban vitality [120] often include numerous multi-source variables without adequately considering their collinearity. Our stepwise VIF-based method aimed at striking a balance between selecting variables that provided comprehensive information, and controlling for their multicollinearity. However, there are inherent trade-offs and limitations in our approach. For example, the complex correlations between socio-demographic and environmental factors are difficult to quantify, and their impact on the model’s predictions is challenging to measure [88]. Therefore, the VIF threshold and the amount of information in urban characteristics are extremely difficult to determine. Traditional ablation studies assess model component redundancy and impact [85], often overlooking spatial hyper-parameters. In this study, we addressed this gap by holistically considering spatial and topological components, including the construction of the spatial network graph, the GNN architecture, and the positional/location encoding method. Given the computational constraints, we employed a local sequential ablation study, testing only a subset of component combinations — a limitation future research should address for example through neural architectural search [126]. Notably, MedGNN’s target-agnostic architecture makes it applicable for different neighbourhood-level prediction tasks including energy consumption or house prices.

### 4.2 Explainability through PCA Interpretation

The PCA1 component in Figure 4, accounting for over 61% of the variance in socio-demographic and urban characteristics, reveals a clear gradient from central London to the suburbs, which differ significantly in key attributes [3, 50]. In contrast, PCA2, explaining another 24% of variance, highlights deviations in antidepressant prescription (see Figure 3)

from the centre-suburb pattern observed in the PCA1 heatmap. PCA2 identifies central areas with unexpectedly high prescriptions, and is primarily linked to ethnicity, with higher PCA2 values associated with White and lower with Asian on the opposite sides of the spectrum. A linear regression model using PCA1 and PCA2 predicts antidepressant prescriptions with an  $R^2$  exceeding 0.90, indicating that the extracted components capture key spatial and structural patterns. The coefficients also show that both dimensions are positively associated with antidepressants. Based on the PCA correlations with different neighbourhood characteristics, we categorized findings into three groups: those aligning with existing literature, those contributing to ongoing debates, and insights not previously reported that potentially warrant future research.

*4.2.1 Alignment with literature.* Our model reveals nuanced relationships between age and antidepressant prescriptions. Higher prescription rates are observed among both the elderly [20] and younger populations aged 10 to 19 [7, 70]. In contrast, lower prescription rates are associated with individuals aged 20 to 39, who are more likely to commute by bicycle [13] or on foot [104], work in professional occupations [96], and, notably, work from home—a factor shown to protect mental health, particularly during COVID [16]. The strongest correlation for PCA1 is with under-occupied rooms (0.53), likely reflecting loneliness [35]. Additionally, both PCA1 and PCA2 correlate with the White population ( $> 0.30$ ), a previously reported trend for antidepressants [102]. Notably, lower prescription rates are associated with Muslim communities, recent immigrants, and individuals with limited English proficiency. Prior research suggests that Christian communities in older architectural areas exhibit different prescription patterns than newer immigrant communities in apartment buildings [8, 79, 110]. Since our data reflect prescriptions rather than prevalence, limited English proficiency may act as a barrier to accessing antidepressants [73]. Figures 4 A-D illustrate street views of these distinct communities.

*4.2.2 Adding to the debate.* We find a positive association between antidepressant prescriptions and green, crop, and shrub land cover. While most studies suggest a lower incidence of depression in relation to greenery [19], some have also reported the unexpected positive link observed here [9, 54]. Interestingly, working more than 49 hours per week—exceeding the UK Working Time Directive<sup>1</sup>—correlates with lower antidepressant prescriptions ( $-0.29$  with PCA1). This contradicts research linking excessive workload and job stress to depression [84] but may simply indicate that employment itself is associated with greater well-being. It also aligns with studies highlighting potential positive aspects of work-related stress [99]. Additionally, we find a strong negative correlation between  $\text{NO}_2$  levels and antidepressant use. While prior studies report a positive link between poor air quality and mental health issues [76], similar negative correlations have been observed in other datasets [39] as well as in MEDSAT [82, 116]. In London, this relationship may be influenced by the Ultra Low Emission Zone (ULEZ) policy, gradually introduced since 2019<sup>2</sup>.

*4.2.3 Insights calling for future research.* By applying MedGNN to this rich dataset, we were able to analyze a broader range of factors than is typical in public health studies. As a result, we identified associations that have not been previously explored in this context but potentially warrant future research. These include associations between increased antidepressant prescriptions and commuting by train, as well as employment in caring and leisure occupations. Additionally, we find that the environmental factors total runoff (refers to the total volume of water that flows over land surfaces into streams, rivers, and other water bodies after precipitation) and canopy evaporation are linked to lower antidepressants. For example, total runoff could be higher in areas with better-managed water infrastructure, often

<sup>1</sup><https://www.gov.uk/maximum-weekly-working-hours>

<sup>2</sup><https://tfl.gov.uk/modes/driving/ultra-low-emission-zone>

associated with greener, more walkable environments that promote well-being. More tree cover of specific types leads to increased canopy evaporation, cooling urban areas and potentially reducing heat-related stress and discomfort. The insights uncovered by MedGNN highlight the potential of AI-driven models, particularly those integrating explainability and interpretability, to reveal previously overlooked relationships in public health. Transdisciplinary collaborations with public health and urban experts could allow to design targeted studies that validate these hypotheses and further leverage machine learning for advancing individualized and data-driven public health research.

## 5 Related Work

*Urban socio-demographic and Environmental Correlates of Health.* Previous studies have linked environmental and socio-demographic features to health outcomes. For instance, Kihal-Talantikite et al. [61] found that low-income populations in environmentally disadvantaged areas face compounded health risks, particularly in highly unequal regions. Similarly, Zhou et al. [127] demonstrated the benefits of green and blue spaces in mitigating hypertension risks. Research from [83, 113, 118] further underscored the associations between depression, diabetes, and environmental characteristics. However, these studies often focus on isolated factors such as greenery, rather than the broader context of urban health disparities, potentially overlooking complex interactions across urban systems.

*Machine Learning Applications in Health Research.* The integration of large-scale datasets in health research has introduced new challenges in handling multidimensional characteristics, such as those derived from Remote Sensing (RS) data [92]. While statistical models were traditionally used to analyze health outcomes [97, 103], their reliance on explicit assumptions and prior knowledge makes them less suitable for high-dimensional and nonlinear data [93, 105]. For instance, Lalloué et al. [71] highlighted the limitations of statistical models in addressing complex and nonlinear urban health patterns. In contrast, Machine Learning (ML) methods have shown significant advantages in health prediction tasks due to their flexibility and ability to handle complex data without strict assumptions [57]. Studies from [14, 106, 109] have successfully used ML models to predict incidence of depression, diabetes, and hypertension. However, ML models often struggle to incorporate geographic context, as noted by Arcaya et al. [6] and Sarkar and Webster [98], limiting their ability to address spatial heterogeneity and dependency. Furthermore, these models frequently lack spatial interpretability, a critical issue in geo-health research.

*GeoAI and GNNs in Health Research.* Furthermore, there is a growing body of work examining the relationship between urban spatial heterogeneity and health inequalities [112]. Researchers have increasingly emphasized the importance of spatial context and environmental exposure in health research, particularly following the COVID-19 pandemic [68, 75]. GeoAI, which focuses on developing spatially explicit AI models integrating GIS and AI advances, has emerged as a promising approach in health research [64, 81, 101, 115]. Among GeoAI methods, GNNs stand out for their ability to model spatial relationships, capture geographic and social connections in urban environments [65, 74, 122] and analyze disease transmission [26]. Helbich [52] emphasized the importance of integrating multi-source spatial data for analyzing health inequalities, while Tung et al. [112] highlighted the relevance of urban spatial heterogeneity and dependency in understanding health risks. Despite GNN's ability to capture spatial interaction [32, 81], the application of GNNs in urban health research remains limited partially due to its black-box nature. While studies like Lu and Uddin [80] and Fritz et al. [42] have explored disease prediction using GNNs, most focus on algorithmic improvements and epidemiological investigation, few analysed urban health disparities and on interpreting its drivers. Bridging this gap,

our framework offers significant potential for predicting health prescriptions by capturing complex spatial patterns and socio-economic influences at the community level [74].

## 6 Conclusion

This study investigates the use of machine learning and AI methods in public health [86], and demonstrates the effectiveness of spatio-topologically explicit graph neural network (MedGNNs) in predicting health outcomes at the community level by leveraging socio-demographic and environmental data. Compared to other baselines, our MedGNN excelled in capturing complex spatial dependencies and integrating multidimensional urban characteristics, achieving superior performance across all prescriptions. Through ten-fold cross-validation and leave-one-out analysis, MedGNN model showcased strong generalization and robustness in diverse urban settings. Residual visualisations further highlighted the model's accuracy, while PCA-based explanations validate prior health studies and offered valuable insights into potentially more complex socio-demographic and environmental drivers.

## References

- [1] N. O. Adeboye, I. S. Fagoyinbo, and T. O. Olatayo. Estimation of the effect of multicollinearity on the standard error for regression coefficients. *Journal of Mathematics*, 10(4):16–20, 2014.
- [2] M. Adnan, A. A. S. Alarood, M. I. Uddin, and I. ur Rehman. Utilizing grid search cross-validation with adaptive boosting for augmenting performance of machine learning models. *PeerJ Computer Science*, 8:e803, 2022.
- [3] Luca Maria Aiello, Rossano Schifanella, Daniele Quercia, and Lucia Del Prete. Large-scale and high-resolution analysis of food purchases and health outcomes. *EPJ Data Science*, 8(1):1–22, 2019.
- [4] Margarita Alegría, Amanda NeMoyer, Irene Falgás Bagué, Ye Wang, and Kiara Alvarez. Social determinants of mental health: where we are and where we need to go. *Current psychiatry reports*, 20:1–13, 2018.
- [5] Luc Anselin. Spatial regression. *The SAGE handbook of spatial analysis*, 1:255–276, 2009.
- [6] M. C. Arcaya, R. D. Tucker-Seeley, R. Kim, A. Schnake-Mahl, M. So, and S. V. Subramanian. Research on neighborhood effects on health in the united states: a systematic review of study characteristics. *Social Science & Medicine*, 168:16–29, 2016.
- [7] Richard Armitage. Antidepressants, primary care, and adult mental health services in england during covid-19. *The Lancet Psychiatry*, 8(2):e3, 2021.
- [8] S. Assari. Social determinants of depression: The intersections of race, gender, and socioeconomic status. *Brain Sciences*, 7(12):156, 2017.
- [9] Thomas Astell-Burt, Michael Navakatikyan, Simon Eckermann, Maree Hackett, and Xiaoqi Feng. Is urban green space associated with lower mental healthcare expenditure? *Social Science & Medicine*, 292:114503, 2022.
- [10] J. E. Bell, C. L. Brown, K. Conlon, S. Herring, K. E. Kunkel, J. Lawrimore, and C. Uejio. Changes in extreme events and the potential impacts on human health. *Journal of the Air & Waste Management Association*, 68(4):265–287, 2018.
- [11] David A Belsley, Edwin Kuh, and Roy E Welsch. *Regression diagnostics: Identifying influential data and sources of collinearity*. John Wiley & Sons, 2005.
- [12] Tami D Benton, Rhonda C Boyd, and Wanjikū FM Njoroge. Addressing the global crisis of child and adolescent mental health. *JAMA pediatrics*, 175(11):1108–1110, 2021.
- [13] Laurie Berrie, Zhiqiang Feng, David Rice, Tom Clemens, Lee Williamson, and Chris Dibben. Does cycle commuting reduce the risk of mental ill-health? an instrumental variable analysis using distance to nearest cycle path. *International journal of epidemiology*, 53(1):dyad153, 2024.
- [14] I. Bhakta and A. Sau. Prediction of depression among senior citizens using machine learning classifiers. *International Journal of Computer Applications*, 144(7):11–16, 2016.
- [15] U. A. Bhatti, H. Tang, G. Wu, S. Marjan, and A. Hussain. Deep learning with graph convolutional networks: An overview and latest applications in computational intelligence. *International Journal of Intelligent Systems*, 2023(1):8342104, 2023.
- [16] Luca Bonacini, Giovanni Gallo, and Sergio Scicchitano. Working from home and income inequality: risks of a ‘new normal’ with covid-19. *Journal of population economics*, 34(1):303–360, 2021.
- [17] William Bor, Angela J Dean, Jacob Najman, and Reza Hayatbakhsh. Are child and adolescent mental health problems increasing in the 21st century? a systematic review. *Australian & New Zealand journal of psychiatry*, 48(7):606–616, 2014.
- [18] S. Brody, U. Alon, and E. Yahav. How attentive are graph attention networks? *arXiv preprint arXiv:2105.14491*, 2021.
- [19] M. H. Browning, K. Lee, and K. L. Wolf. Tree cover shows an inverse relationship with depressive symptoms in elderly residents living in us nursing homes. *Urban Forestry & Urban Greening*, 41:23–32, 2019.
- [20] Cynthia G Cahoon. Depression in older adults. *AJN The American Journal of Nursing*, 112(11):22–30, 2012.
- [21] S. Capolongo, A. Rebecchi, M. Buffoli, L. Appolloni, C. Signorelli, G. M. Fara, and D. D’Alessandro. Covid-19 and cities: From urban health strategies to the pandemic challenge. a decalogue of public health opportunities. *Acta Bio Medica: Atenei Parmensis*, 91(2):13, 2020.
- [22] J. Y. L. Chan, S. M. H. Leow, K. T. Bea, W. K. Cheng, S. W. Phoong, Z. W. Hong, and Y. L. Chen. Mitigating the multicollinearity problem and its machine learning approach: a review. *Mathematics*, 10(8):1283, 2022.
- [23] Y. Chen, L. Wu, and M. Zaki. Iterative deep graph learning for graph neural networks: Better and robust node embeddings. In *Advances in Neural Information Processing Systems*, volume 33, pages 19314–19326, 2020.
- [24] Y. Chen, J. You, J. He, Y. Lin, Y. Peng, C. Wu, and Y. Zhu. Sp-gnn: Learning structure and position information from graphs. *Neural Networks*, 161: 505–514, 2023.
- [25] J. Cheng, J. Sun, K. Yao, M. Xu, and Y. Cao. A variable selection method based on mutual information and variance inflation factor. *Spectrochimica Acta Part A: Molecular and Biomolecular Spectroscopy*, 268:120652, 2022.
- [26] E. Choi, Z. Xu, Y. Li, M. Dusenberry, G. Flores, E. Xue, and A. Dai. Learning the graphical structure of electronic health records with graph convolutional transformer. In *Proceedings of the AAAI Conference on Artificial Intelligence*, pages 606–613. AAAI Press, 2020.
- [27] J. Cohen, P. Cohen, S. G. West, and L. S. Aiken. *Applied multiple regression/correlation analysis for the behavioral sciences*. Routledge, 2013.
- [28] H. V. Cole, R. Mehdipanah, P. Gullón, and M. Triguero-Mas. Breaking down and building up: gentrification, its drivers, and urban health inequality. *Current Environmental Health Reports*, 8:157–166, 2021.
- [29] Michael T Compton and Ruth S Shim. The social determinants of mental health. *Focus*, 13(4):419–425, 2015.
- [30] J. Corburn, D. Vlahov, B. Mberu, L. Riley, W. T. Caiaffa, S. F. Rashid, and H. Ayad. Slum health: arresting covid-19 and improving well-being in urban informal settlements. *Journal of Urban Health*, 97:348–357, 2020.

- [31] Simon Cousens, J Hargreaves, Chris Bonell, B Armstrong, J Thomas, BR Kirkwood, and R Hayes. Alternatives to randomisation in the evaluation of public-health interventions: statistical analysis and causal inference. *Journal of Epidemiology & Community Health*, 65(7):576–581, 2011.
- [32] S. De Sabbata and P. Liu. A graph neural network framework for spatial geodemographic classification. *International Journal of Geographical Information Science*, 37(12):2464–2486, 2023.
- [33] Bruno Samways dos Santos, Maria Teresinha Arns Steiner, Amanda Trojan Fenerich, and Rafael Henrique Palma Lima. Data mining and machine learning techniques applied to public health problems: A bibliometric analysis from 2009 to 2018. *Computers & Industrial Engineering*, 138:106120, 2019.
- [34] V. P. Dwivedi, A. T. Luu, T. Laurent, Y. Bengio, and X. Bresson. Graph neural networks with learnable structural and positional representations. *arXiv preprint arXiv:2110.07875*, 2021. URL <https://arxiv.org/abs/2110.07875>.
- [35] Evren Erzen and Özkan Çikrikci. The effect of loneliness on depression: A meta-analysis. *International Journal of Social Psychiatry*, 64(5):427–435, 2018.
- [36] Daisy Fancourt, Andrew Steptoe, and Feifei Bu. Trajectories of anxiety and depressive symptoms during enforced isolation due to covid-19 in england: a longitudinal observational study. *The Lancet Psychiatry*, 8(2):141–149, 2021.
- [37] J. Feng, Y. Chen, F. Li, A. Sarkar, and M. Zhang. How powerful are k-hop message passing graph neural networks. In *Advances in Neural Information Processing Systems*, volume 35, pages 4776–4790, 2022.
- [38] K. Fiscella and D. R. Williams. Health disparities based on socioeconomic inequities: implications for urban health care. *Academic Medicine*, 79(12):1139–1147, 2004.
- [39] Vanessa Fleury, Rebecca Himsl, Stéphane Joost, Nicolas Nicastro, Matthieu Bereau, Idris Guessous, and Pierre R Burkhard. Geospatial analysis of individual-based parkinson’s disease data supports a link with air pollution: A case-control study. *Parkinsonism & Related Disorders*, 83:41–48, 2021.
- [40] Office for National Statistics (ONS). National statistics, 2025. URL <https://www.ons.gov.uk>.
- [41] A Stewart Fotheringham, Chris Brunsdon, and ME Charlton. Geographically weighted regression. *The Sage handbook of spatial analysis*, 1:243–254, 2009.
- [42] C. Fritz, E. Dorigatti, and D. Rügamer. Combining graph neural networks and spatio-temporal disease models to improve the prediction of weekly covid-19 cases in germany. *Scientific Reports*, 12(1):3930, 2022.
- [43] T. Fushiki. Estimation of prediction error by using k-fold cross-validation. *Statistics and Computing*, 21:137–146, 2011.
- [44] A. Garg and K. Tai. Comparison of statistical and machine learning methods in modelling of data with multicollinearity. *International Journal of Modelling, Identification and Control*, 18(4):295–312, 2013.
- [45] Google Earth Engine (GEE). Google earth engine: A cloud-based platform for earth science data analysis, 2025. URL <https://earthengine.google.com>.
- [46] M. Grant, C. Brown, W. T. Caiaffa, A. Capon, J. Corburn, C. Coutts, and C. Ward Thompson. Cities and health: an evolving global conversation. *Cities & health*, 1(1):1–9, 2017.
- [47] M. Greenacre, P. J. Groenen, T. Hastie, A. I. d’Enza, A. Markos, and E. Tuzhilina. Principal component analysis. *Nature Reviews Methods Primers*, 2(1):100, 2022.
- [48] Will Hamilton, Zhitao Ying, and Jure Leskovec. Inductive representation learning on large graphs. *Advances in neural information processing systems*, 30, 2017.
- [49] Samuel B Harvey, Matthew Modini, Sadhbh Joyce, Josie S Milligan-Saville, Leona Tan, Arnstein Mykletun, Richard A Bryant, Helen Christensen, and Philip B Mitchell. Can work make you mentally ill? a systematic meta-review of work-related risk factors for common mental health problems. *Occupational and Environmental Medicine*, 74(4):301–310, 2017.
- [50] Stephani L Hatch, Souci Frissa, Maria Verdecchia, Robert Stewart, Nicola T Fear, Abraham Reichenberg, Craig Morgan, Bwalya Kankulu, Jennifer Clark, Billy Gazard, et al. Identifying socio-demographic and socioeconomic determinants of health inequalities in a diverse london community: the south east london community health (selcoh) study. *BMC public health*, 11:1–17, 2011.
- [51] Matthew J Hayat, Amanda Powell, Tessa Johnson, and Betsy L Cadwell. Statistical methods used in the public health literature and implications for training of public health professionals. *PloS one*, 12(6):e0179032, 2017.
- [52] M. Helbich. Toward dynamic urban environmental exposure assessments in mental health research. *Environmental Research*, 161:129–135, 2018.
- [53] Md Mahbub Hossain, Samia Tasnim, Abida Sultana, Farah Faizah, Hoimonty Mazumder, Liye Zou, E Lisako J McKyer, Helal Uddin Ahmed, and Ping Ma. Epidemiology of mental health problems in covid-19: a review. *F1000Research*, 9, 2020.
- [54] Roger Hyam. Greenness, mortality and mental health prescription rates in urban scotland—a population level, observational study. *Research Ideas and Outcomes*, 6:e53542, 2020.
- [55] Michaela Hynie. The social determinants of refugee mental health in the post-migration context: A critical review. *The Canadian Journal of Psychiatry*, 63(5):297–303, 2018.
- [56] Scholastica Ijeh, Chioma Anthonia Okolo, Jeremiah Olawumi Arowoogun, Adekunle Oyeyemi Adeniyi, and Olufunke Omotayo. Predictive modeling for disease outbreaks: a review of data sources and accuracy. *International Medical Science Research Journal*, 4(4):406–419, 2024.
- [57] M. I. Jordan and T. M. Mitchell. Machine learning: Trends, perspectives, and prospects. *Science*, 349(6245):255–260, 2015.
- [58] Guolin Ke, Qi Meng, Thomas Finley, Taifeng Wang, Wei Chen, Weidong Ma, Qiwei Ye, and Tie-Yan Liu. Lightgbm: A highly efficient gradient boosting decision tree. *Advances in neural information processing systems*, 30, 2017.
- [59] Michael Kearns and Dana Ron. Algorithmic stability and sanity-check bounds for leave-one-out cross-validation. In *Proceedings of the Tenth Annual Conference on Computational Learning Theory (COLT 1997)*, pages 152–162. ACM, July 1997.

- [60] C. Kedzie, K. McKeown, and H. Daume III. Content selection in deep learning models of summarization. *arXiv preprint arXiv:1810.12343*, 2018.
- [61] Wahida Kihal-Talantikite, Clara M Padilla, Benoit Lalloué, Marcella Gelormini, Denis Zmirou-Navier, and Severine Deguen. Green space, social inequalities and neonatal mortality in france. *BMC Pregnancy and Childbirth*, 13:1–9, 2013.
- [62] T. N. Kipf and M. Welling. Semi-supervised classification with graph convolutional networks. *arXiv preprint arXiv:1609.02907*, 2016.
- [63] T. Kjellstrom. Impact of climate conditions on occupational health and related economic losses: a new feature of global and urban health in the context of climate change. *Asia Pacific Journal of Public Health*, 28(2\_suppl):28S–37S, 2016.
- [64] K. Klemmer, E. Rolf, C. Robinson, L. Mackey, and M. Rußwurm. Satclip: Global, general-purpose location embeddings with satellite imagery. *arXiv preprint arXiv:2311.17179*, 2023.
- [65] Konstantin Klemmer, Nathan S Safir, and Daniel B Neill. Positional encoder graph neural networks for geographic data. In *International Conference on Artificial Intelligence and Statistics*, pages 1379–1389. PMLR, 2023.
- [66] Jude Dzevela Kong, Ugochukwu Ejike Akpudo, Jake Okechukwu Effoduh, and Nicola Luigi Bragazzi. Leveraging responsible, explainable, and local artificial intelligence solutions for clinical public health in the global south. *Healthcare*, 11(4):457, 2023. doi: 10.3390/healthcare11040457.
- [67] T. Kong, T. Kim, J. Jeon, J. Choi, Y. C. Lee, N. Park, and S. W. Kim. Linear, or non-linear, that is the question! In *Proceedings of the Fifteenth ACM International Conference on Web Search and Data Mining*, pages 517–525. ACM, February 2022.
- [68] Kimon Krenz, Ashley Dhanani, Rosemary RC McEachan, Kuldeep Sohal, John Wright, and Laura Vaughan. Linking the urban environment and health: an innovative methodology for measuring individual-level environmental exposures. *International Journal of Environmental Research and Public Health*, 20(3):1953, 2023.
- [69] T. Kyriazos and M. Poga. Dealing with multicollinearity in factor analysis: the problem, detections, and solutions. *Open Journal of Statistics*, 13(3):404–424, 2023.
- [70] Hasnain M Lalji, Anita McGrogan, and Sarah J Bailey. An analysis of antidepressant prescribing trends in england 2015–2019. *Journal of affective disorders reports*, 6:100205, 2021.
- [71] B. Lalloué, J. M. Monnez, C. Padilla, W. Kihal, N. Le Meur, D. Zmirou-Navier, and S. Deguen. A statistical procedure to create a neighborhood socioeconomic index for health inequalities analysis. *International Journal for Equity in Health*, 12:1–11, 2013.
- [72] K. Le Rest, D. Pinaud, P. Monestiez, J. Chadoeuf, and V. Bretagnolle. Spatial leave-one-out cross-validation for variable selection in the presence of spatial autocorrelation. *Global Ecology and Biogeography*, 23(7):811–820, 2014. doi: 10.1111/geb.12135.
- [73] Ira Lesser, Sidney Zisook, Deborah Flores, Andres Sciolla, Stephen Wisniewski, Ian Cook, Marcy Epstein, Aurora Rosales, Carlos Gonzalez, Madhukar Trivedi, et al. Depression outcomes of spanish-and english-speaking hispanic outpatients in star\* d. *Psychiatric Services*, 59(11):1273–1284, 2008.
- [74] M. Li, S. Gao, F. Lu, K. Liu, H. Zhang, and W. Tu. Prediction of human activity intensity using the interactions in physical and social spaces through graph convolutional networks. *International Journal of Geographical Information Science*, 35(12):2489–2516, 2021.
- [75] X. Li, L. Sun, M. Ling, and Y. Peng. A survey of graph neural network based recommendation in social networks. *Neurocomputing*, 549:126441, 2023.
- [76] Y. H. Lim, H. Kim, J. H. Kim, S. Bae, H. Y. Park, and Y. C. Hong. Air pollution and symptoms of depression in elderly adults. *Environmental Health Perspectives*, 120(7):1023–1028, 2012.
- [77] P. Liu, Y. Zhang, and F. Biljecki. Explainable spatially explicit geospatial artificial intelligence in urban analytics. *Environment and Planning B: Urban Analytics and City Science*, 51(5):1104–1123, 2024.
- [78] Z. Liu and C. Liu. The association between urban density and multiple health risks based on interpretable machine learning: A study of american urban communities. *Cities*, 153:105170, 2024.
- [79] K. M. Loewenthal, A. K. MacLeod, and M. Cinnirella. Are women more religious than men? gender differences in religious activity among different religious groups in the uk. *Personality and Individual Differences*, 32(1):133–139, 2002.
- [80] H. Lu and S. Uddin. A weighted patient network-based framework for predicting chronic diseases using graph neural networks. *Scientific Reports*, 11(1):22607, 2021.
- [81] G. Mai, K. Janowicz, B. Yan, R. Zhu, L. Cai, and N. Lao. Multi-scale representation learning for spatial feature distributions using grid cells. *arXiv preprint arXiv:2003.00824*, 2020.
- [82] I. Maitra, R. Lin, E. Chen, J. Donnelly, S. Šćepanović, and C. Rudin. How your location relates to health: Variable importance and interpretable machine learning for environmental and sociodemographic data. *arXiv preprint arXiv:2501.02111*, 2025.
- [83] Sharmistha Mazumdar, Sylvia Chong, Thomas Astell-Burt, Xiaoqi Feng, Geoff Morgan, and Bin Jalaludin. Which green space metric best predicts a lowered odds of type 2 diabetes? *International Journal of Environmental Research and Public Health*, 18(8):4088, 2021.
- [84] Maria Melchior, Avshalom Caspi, Barry J Milne, Andrea Danese, Richie Poulton, and Terrie E Moffitt. Work stress precipitates depression and anxiety in young, working women and men. *Psychological medicine*, 37(8):1119–1129, 2007.
- [85] R. Meyes, M. Lu, C. W. de Puiseau, and T. Meisen. Ablation studies in artificial neural networks. *arXiv preprint arXiv:1901.08644*, 2019.
- [86] Vishwali Mhasawade, Yuan Zhao, and Rumi Chunara. Machine learning and algorithmic fairness in public and population health. *Nature Machine Intelligence*, 3(8):659–666, 2021.
- [87] Christoph Molnar, Gunnar König, Julia Herbringer, Timo Freiesleben, Susanne Dandl, Christian A Scholbeck, Giuseppe Casalicchio, Moritz Grosse-Wentrup, and Bernd Bischl. Pitfalls to avoid when interpreting machine learning models. <https://arxiv.org/abs/2007.04131>, 2020. *arXiv preprint arXiv:2007.04131*.

- [88] A. Mondini and F. Chiaravalloti-Neto. Spatial correlation of incidence of dengue with socioeconomic, demographic and environmental variables in a brazilian city. *Science of the Total Environment*, 393(2-3):241–248, 2008.
- [89] Andrew Y. Ng. Preventing "overfitting" of cross-validation data. In *Proceedings of the 14th International Conference on Machine Learning (ICML 1997)*, pages 245–253. Morgan Kaufmann, July 1997.
- [90] National Health Service (NHS). Nhs health data, 2025. URL <https://www.nhs.uk>.
- [91] N. Obradovich, R. Migliorini, M. P. Paulus, and I. Rahwan. Empirical evidence of mental health risks posed by climate change. *Proceedings of the National Academy of Sciences*, 115(43):10953–10958, 2018.
- [92] H. Ohanyan, L. Portengen, O. Kaplani, A. Huss, G. Hoek, J. W. Beulens, and R. Vermeulen. Associations between the urban exposome and type 2 diabetes: Results from penalised regression by least absolute shrinkage and selection operator and random forest models. *Environment International*, 170:107592, 2022.
- [93] H. Pineo, K. Glonti, H. Rutter, N. Zimmermann, P. Wilkinson, and M. Davies. Urban health indicator tools of the physical environment: a systematic review. *Journal of Urban Health*, 95:613–646, 2018.
- [94] M. C. Popescu, V. E. Balas, L. Perescu-Popescu, and N. Mastorakis. Multilayer perceptron and neural networks. *WSEAS Transactions on Circuits and Systems*, 8(7):579–588, 2009.
- [95] RDocumentation. Vif: Variance inflation factor. <https://www.rdocumentation.org/packages/regclass/versions/1.6/topics/VIF>, 2023. Accessed: 2023-03-15.
- [96] Olivia Remes, João Francisco Mendes, and Peter Templeton. Biological, psychological, and social determinants of depression: a review of recent literature. *Brain sciences*, 11(12):1633, 2021.
- [97] R. Rothenberg, S. R. Weaver, D. Dai, C. Stauber, A. Prasad, and M. Kano. A flexible urban health index for small area disparities. *Journal of Urban Health*, 91(5):823–835, 2014.
- [98] C. Sarkar and C. Webster. Urban environments and human health: Current trends and future directions. *Current Opinion in Environmental Sustainability*, 25:33–44, 2017.
- [99] Sanja Šćepanović, Marios Constantinides, Daniele Quercia, and Seunghyun Kim. Quantifying the impact of positive stress on companies from online employee reviews. *Scientific Reports*, 13(1):1603, 2023.
- [100] M. T. Schaub, A. R. Benson, P. Horn, G. Lippner, and A. Jadbabaie. Random walks on simplicial complexes and the normalized hodge 1-laplacian. *SIAM Review*, 62(2):353–391, 2020.
- [101] S. Scheider and K. F. Richter. Pragmatic geoai: Geographic information as externalized practice. *KI-Künstliche Intelligenz*, 37(1):17–31, 2023.
- [102] David A Sclar, Linda M Robison, and Tracy L Skaer. Ethnicity/race and the diagnosis of depression and use of antidepressants by adults in the united states. *International clinical psychopharmacology*, 23(2):106–109, 2008.
- [103] A. M. Shane and T. E. Graedel. Urban environmental sustainability metrics: a provisional set. *Journal of Environmental Planning and Management*, 43(5):643–663, 2000.
- [104] Eetu Soini, Tom Rosenström, Ilmari Määttänen, and Markus Jokela. Physical activity and specific symptoms of depression: A pooled analysis of six cohort studies. *Journal of Affective Disorders*, 348:44–53, 2024.
- [105] X. Song, A. Mitnitski, J. Cox, and K. Rockwood. Comparison of machine learning techniques with classical statistical models in predicting health outcomes. In *MEDINFO 2004*, pages 736–740. IOS Press, 2004.
- [106] D. Su, X. Zhang, K. He, and Y. Chen. Use of machine learning approach to predict depression in the elderly in china: a longitudinal study. *Journal of Affective Disorders*, 282:289–298, 2021.
- [107] R. Sun, H. Dai, and A. W. Yu. Does gnn pretraining help molecular representation? In *Advances in Neural Information Processing Systems*, volume 35, pages 12096–12109, 2022.
- [108] Christine M Thomas and Stephen Morris. Cost of depression among adults in england in 2000. *The British Journal of Psychiatry*, 183(6):514–519, 2003.
- [109] P. N. Thotad, G. R. Bharamagoudar, and B. S. Anami. Diabetes disease detection and classification on indian demographic and health survey data using machine learning methods. *Diabetes & Metabolic Syndrome: Clinical Research & Reviews*, 17(1):102690, 2023.
- [110] S. K. Tiwari and J. Wang. Ethnic differences in mental health service use among white, chinese, south asian and south east asian populations living in canada. *Social Psychiatry and Psychiatric Epidemiology*, 43:866–871, 2008.
- [111] T. Trushna, V. Dhiman, D. Raj, and R. R. Tiwari. Effects of ambient air pollution on psychological stress and anxiety disorder: a systematic review and meta-analysis of epidemiological evidence. *Reviews on Environmental Health*, 36(4):501–521, 2021.
- [112] E. L. Tung, K. A. Cagney, M. E. Peek, and M. H. Chin. Spatial context and health inequity: reconfiguring race, place, and poverty. *Journal of Urban Health*, 94:757–763, 2017.
- [113] Jenna Van Draanen, Calvin Tsang, Saakshi Mitra, Mohammad Karamouzian, and Lindsey Richardson. Socioeconomic marginalization and opioid-related overdose: a systematic review. *Drug and alcohol dependence*, 214:108127, 2020.
- [114] D. Vlahov and S. Galea. Urbanization, urbanicity, and health. *Journal of Urban Health*, 79:S1–S12, 2002.
- [115] T. VoPham, J. E. Hart, F. Laden, and Y. Y. Chiang. Emerging trends in geospatial artificial intelligence (geoai): potential applications for environmental epidemiology. *Environmental Health*, 17:1–6, 2018.
- [116] Sanja Šćepanović, Ivica Obadic, Sagar Joglekar, Laura Giustarini, Cristiano Nattero, Daniele Quercia, and Xiaoxiang Zhu. Medsat: A public health dataset for england featuring medical prescriptions and satellite imagery. *Advances in Neural Information Processing Systems*, 36, 2024.

- [117] H. Wang, H. Yin, M. Zhang, and P. Li. Equivariant and stable positional encoding for more powerful graph neural networks. *arXiv preprint arXiv:2203.00199*, 2022. URL <https://arxiv.org/abs/2203.00199>.
- [118] Mathew P. White, Lewis R. Elliott, James Grellier, Tonia Economou, Sarah Bell, Gregory N. Bratman, and Lora E. Fleming. Associations between green/blue spaces and mental health across 18 countries. *Scientific Reports*, 11(1):8903, 2021.
- [119] T. T. Wong. Performance evaluation of classification algorithms by k-fold and leave-one-out cross validation. *Pattern Recognition*, 48(9):2839–2846, 2015.
- [120] C. Wu, M. Zhao, and Y. Ye. Measuring urban nighttime vitality and its relationship with urban spatial structure: A data-driven approach. *Environment and Planning B: Urban Analytics and City Science*, 50(1):130–145, 2023.
- [121] S. Wu, F. Sun, W. Zhang, X. Xie, and B. Cui. Graph neural networks in recommender systems: a survey. *ACM Computing Surveys*, 55(5):1–37, 2022.
- [122] Y. Wu, D. Zhuang, A. Labbe, and L. Sun. Inductive graph neural networks for spatiotemporal kriging. In *Proceedings of the AAAI Conference on Artificial Intelligence*, pages 4478–4485. AAAI Press, 2021.
- [123] P. K. Yeh, H. W. Chen, and M. S. Chen. Random walk conformer: Learning graph representation from long and short range. In *Proceedings of the AAAI Conference on Artificial Intelligence*, pages 10936–10944. AAAI Press, 2023.
- [124] S. Zhang, H. Tong, J. Xu, and R. Maciejewski. Graph convolutional networks: a comprehensive review. *Computational Social Networks*, 6(1):1–23, 2019.
- [125] Y. Zhang, P. Liu, and F. Biljecki. Knowledge and topology: A two layer spatially dependent graph neural networks to identify urban functions with time-series street view image. *ISPRS Journal of Photogrammetry and Remote Sensing*, 198:153–168, 2023.
- [126] K. Zhou, X. Huang, Q. Song, R. Chen, and X. Hu. Auto-gnn: Neural architecture search of graph neural networks. *Frontiers in Big Data*, 5:1029307, 2022.
- [127] Wei Zhou, Qi Wang, Rong Li, Abliz Kadier, Wenjing Wang, Feifei Zhou, and Li Ling. Combined effects of heatwaves and air pollution, green space and blue space on the incidence of hypertension: a national cohort study. *Science of The Total Environment*, 867:161560, 2023.

## 7 Appendix

### A Control Variables for VIF iteration

Table 3. Control Variables in the Model

Variable Name	Description
Percent Aged 10 to 14	Proportions of the population in different age groups
Percent Aged 15 to 19	
Percent Aged 20 to 24	
...	
Percent Aged 75 to 79	
Percent Aged 80 to 84	
Percent Aged 85+	
Percent Male	Male proportion
Percent Mixed	Mixed-race population ratio
Percent White	White population ratio
Percent Professional	Professional occupation ratio
Population Density	Population density
NDVI	Normalized difference vegetation index
NO2	Nitrogen oxide index
Water	Water body coverage ratio
Trees	Tree coverage ratio
Grass	Grassland coverage ratio
Bare	Bare land coverage ratio

## B Reproducibility

### B.1 Parameter Space for Random Search

Table 4. Hyperparameter search space for random search. The table lists the ranges and options for each hyperparameter used to optimize the GNN model.

Hyperparameter	Search Space
Learning Rate (lr)	{0.001, 0.005, 0.01}
Weight Decay	{1e-4, 5e-4, 1e-3}
Hidden Layer 1 Size (hidden1)	{64, 128, 256}
Hidden Layer 2 Size (hidden2)	{16, 32, 64}
Dropout Rate	{0.1, 0.3, 0.5}
Number of Epochs (num_epochs)	{200, 300}
Optimizer	{adam, sgd, rmsprop}
Early Stopping Patience (patience)	{10, 20}

### B.2 Applied MedSAT Variables and VIF Results

Table 5. VIF Values for Selected Variables

Variable	VIF	Variable	VIF	Variable	VIF
Age 10-14	65.02	Age 55-59	54.52	Age 75-79	27.83
Age 15-19	25.15	Age 60-64	45.78	Age 80-84	20.59
Age 20-24	44.67	Age 65-69	38.94	Age 85+	11.00
Age 25-29	56.72	Age 70-74	35.93	Mixed	31.92
Age 30-34	82.44	White	749.69	Professional Occupations	128.98
Age 35-39	102.99	Population Density	6.96	NO2 Levels	1251.38
Age 40-44	90.65	NDVI	97.65	Water	6.55
Age 45-49	69.26	Trees	8.29	Grass	18.56
Age 50-54	59.19	Bare Land	57.86	Asian	93.86
Male	830.85	Black	67.95	Buddhist	3.43
Muslim	14.37	No Central Heating	9.02	Communal Heating	2.18
Travel For Work < 2km	36.23	49+ Hours Worked	41.01	Commute on Foot	33.41
Commute Metro Rail	14.83	Commute by Bus	24.62	Commute by Bicycle	10.18
Students	5.76	Highly Under Occupied Rooms	8.58	Under Occupied Rooms	34.75
Lives Here 10+ Years	104.87	Lives Here 2-5 Years	23.39	Lives Here 5-10 Years	31.33
Married or Partnership	2.94	Separated	1.20	Divorced	1.61
Cannot Speak English Well	26.36	Cannot Speak English	7.16	Highly Deprived	2.65
Christian	87.08	Works From Home	288.15	Works Part Time	132.25
Commute by Train	11.21	Moved to the UK From Abroad	7.44	Highly Over Occupied Rooms	31.00
Technical Occupations	101.84	Skilled Trades Occupations	39.09	Caring and Leisure Occupations	47.45
Divorced	47.86	Lake Mixing Depth	103.65	Snow Cover	53.41
Total Runoff	185.38	Snow and Ice Cover	53.98	Crops Cover	14.98
Canopy Evaporation	347.74	Shrub Cover	108.23		

### B.3 Hardware and Software Requirements

Table 6. Hardware and Software Configuration

Hardware Component	Specification	Software/Package	Version
Operating System	Windows 10 (Version 10.0.22631)	Python	3.11.7 (Anaconda)
CPU Model	Intel Core i9-13900K (16 Cores, 24 Threads)	PyTorch	2.0.0+cu117
Memory	31.82 GB (Total)	NumPy	1.23.5
GPU Model	NVIDIA GeForce RTX 4090	pandas	2.0.3
Available Memory	15.96 GB	Geopandas	0.13.0
Used Memory	15.86 GB	NetworkX	2.8.4
GPU Memory Allocated	0 bytes (Check in code)	Torch-Geometric	2.6.1
GPU Memory Cached	0 bytes (Check in code)	Scikit-learn	1.1.2

## C Further Methodological Details

### C.1 LSOAs and Geographical Distribution for LOOCV

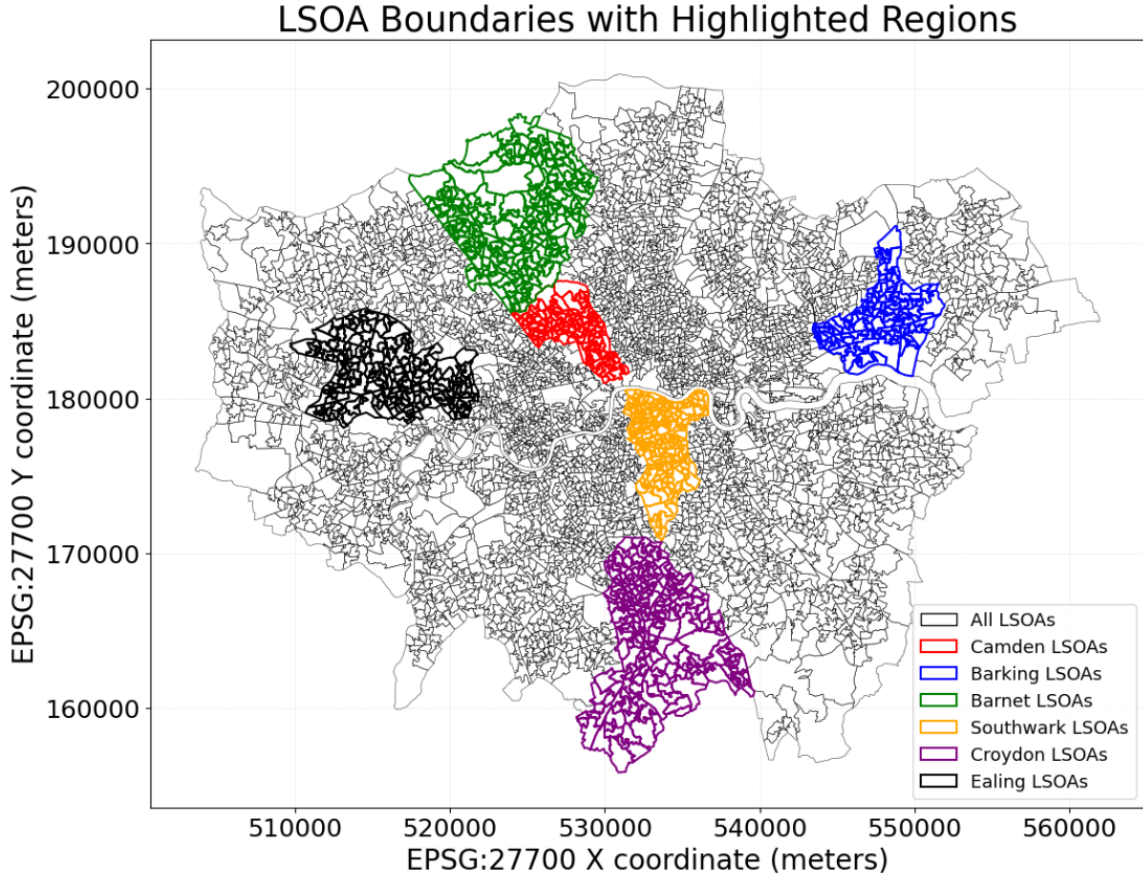


Fig. 5. Highlighted LSOA boundaries for six selected Boroughs regions used in LOOCV: Camden, Barking, Barnet, Southwark, Croydon and Ealing.

### C.2 Baseline Models

Following previous literature [116], three baseline models have been selected as comparison namely, Spatial Lag Model (SLM), Geographically Weighted Regression (GWR), and LightGBM. SLM[5] accounts for spatial dependence by incorporating a spatially lagged dependent variable, capturing interactions among neighbouring observations. GWR[41] extends traditional regression by allowing spatially varying coefficients, enabling localised relationship modelling. LightGBM[58], on the otherhand is an efficient ensemble gradient boosting method.

### C.3 GNNs and Message Passing Mechanisms

This section will more formally defined GNN and its various architecture. A graph is defined as  $G = (\mathcal{V}, \mathcal{E})$ , where  $\mathcal{V}$  is the set of nodes/vertices (eg. in this case geographical regions such as LSOA), and  $\mathcal{E}$  is the set of edges connecting

pairs of nodes (eg. in this case adjacent geographical regions). The connectivity of the graph can be represented by an *adjacency matrix*  $A \in \mathbb{R}^{|\mathcal{V}| \times |\mathcal{V}|}$ , where:

$$A_{ij} = \begin{cases} 1, & \text{if there is an edge between nodes } v_i \text{ and } v_j \\ 0, & \text{otherwise.} \end{cases}$$

Each node  $v_i$  is associated with a feature vector  $\mathbf{h}_i$ , which serves as the input for learning node representations in a GNN. A generic GNNs[62] can then be defined as:

$$\mathbf{h}_i^{(l+1)} = \mathcal{U}\left(\mathbf{h}_i^{(l)}, \mathcal{M}\left(\{\mathbf{h}_j^{(l)} \mid v_j \in \mathcal{N}(i)\}\right)\right)$$

Where  $\mathbf{h}_i^{(l)}$  denotes the feature vector of node  $i$  at layer  $l$ , and  $\mathcal{M}$  aggregates information from neighbouring nodes  $\mathcal{N}(i)$ , while  $\mathcal{U}$  combines the aggregated information with the node's own feature vector to produce the updated node feature. This formulation generalises GNN architectures by abstracting the message passing and update steps where different GNN architectures implement different aggregation and update mechanisms.

Graph Convolutional Neural Network GCN use a linear combination of the adjacency matrix and node features for information aggregation, as shown by the formula:

$$\mathbf{h}_i^{(l+1)} = \sigma\left(\sum_{j \in \mathcal{N}(i)} \hat{A}_{ij} \mathbf{W}^{(l)} \mathbf{h}_j^{(l)}\right)$$

Here,  $\hat{A}_{ij}$  is the normalized adjacency matrix,  $\mathbf{W}^{(l)}$  is the weight matrix, and  $\sigma$  is a non-linear activation function. This approach aggregates information from neighboring nodes linearly, making it effective for tasks where node relationships are simple and linearly correlated [67]. In contrast, Graph Isomorphism Network GIN employs a multi-layer perceptron (MLP) to perform non-linear aggregation of node features [94], with the update rule:

$$\mathbf{h}_i^{(l+1)} = \text{MLP}\left((1 + \epsilon^{(l)})\mathbf{h}_i^{(l)} + \sum_{j \in \mathcal{N}(i)} \mathbf{h}_j^{(l)}\right)$$

This non-linear aggregation enables GIN to capture more complex relationships, making it suitable for tasks with intricate dependencies between nodes. GraphSAGE, on the other hand, extends the idea of neighborhood aggregation by sampling a fixed-size subset of neighbors and applying an aggregation function (e.g., mean, LSTM, or pooling) [48]. The update rule for GraphSAGE is given by:

$$\mathbf{h}_i^{(l+1)} = \sigma\left(\mathbf{W}^{(l)} \cdot \text{CONCAT}\left(\mathbf{h}_i^{(l)}, \text{AGGR}\left(\{\mathbf{h}_j^{(l)} \mid v_j \in \mathcal{S}(i)\}\right)\right)\right)$$

Here,  $\mathcal{S}(i)$  denotes a sampled subset of neighbors for node  $i$ , and AGGR is a function that aggregates the features of the sampled neighbors. This approach allows GraphSAGE to scale to large graphs by reducing the computational complexity of neighborhood aggregation.

Graph Attention Network V2 GATv2, on the other hand, uses an attention mechanism to assign different weights to neighboring nodes. The update rule for GATv2 is given by:

$$\mathbf{h}_i^{(l+1)} = \sigma\left(\sum_{j \in \mathcal{N}(i)} \text{LeakyReLU}\left(\mathbf{a}^{(l)}(\mathbf{W}^{(l)} \mathbf{h}_i^{(l)} \parallel \mathbf{W}^{(l)} \mathbf{h}_j^{(l)})\right)\right),$$

where  $\mathbf{a}^{(l)}$  represents the attention coefficients, and  $\parallel$  denotes concatenation. The attention mechanism allows the model to focus on the most relevant neighboring nodes, making it particularly effective for capturing complex relationships in the graph structure [18].

#### C.4 Positional Encoding

The specific Laplace embedding process is as follows:

$$\mathbf{h}_i = \sum_{j \in \mathcal{N}(i)} (A_{ij} \cdot \mathbf{h}_j + \lambda \cdot \mathbf{x}_i)$$

where:  $\mathcal{N}(i)$  represents the set of neighbors of node  $i$ ,  $\mathbf{x}_i$  is the original feature of node  $i$ .  $\mathbf{h}_i$  is the updated embedding of node  $i$ .  $\lambda$  is the balancing factor used to control the weight of the original feature, which is '1' here because we regard all nodes as equally weighted.

The representation of random walk probabilistic embedding is:

$$P(v_i, t) = \frac{1}{Z} \sum_{j \in \mathcal{N}(v_i)} \frac{A_{ij}}{d_i} P(v_j, t-1)$$

where:  $P(v_i, t)$  is the probability distribution of node  $v_i$  at time  $t$ .  $A_{ij}$  is the adjacency matrix element, representing the connection between node  $v_i$  and node  $v_j$ .  $d_i$  is the degree of node  $v_i$ .  $Z$  is a normalization factor to ensure that the probability distribution sums to 1.